# Molecular Dynamics Simulation To Investigate Differences in Minor Groove Hydration of HNA/RNA Hybrids As Compared to HNA/DNA Complexes

**H. De Winter,† E. Lescrinier, A. Van Aerschot, and P. Herdewijn***

*Contribution from the Laboratory of Medicinal Chemistry, Rega Institute, Catholic University of Leuven, Minderbroedersstraat 10, B-3000 Leuven, Belgium*

*Received October 27, 1997*

**Abstract:** Hexitol nucleic acids (HNA) are oligonucleotides built up from natural nucleobases and a phosphorylated 1,5-anhydrohexitol backbone. Molecular associations between HNA and RNA are more stable than between HNA and DNA and between natural nucleic acids (dsDNA, dsRNA, DNA/RNA). $^1$H NMR analysis of a HNA dimer confirms the axial orientation of the base moiety with respect to the hexitol ring, and this was used as starting conformation for a molecular dynamics study of HNA/RNA and HNA/DNA duplexes. Both complexes show an A-type geometry and very similar hydrogen bonding patterns between base pairs. The relative stability of HNA/RNA versus HNA/DNA might be explained by a difference in minor groove solvatation.

## Introduction

Hexitol nucleic acids (HNA) represent a new oligomeric structure able to hybridize sequence selectively as well with DNA, RNA, and with itself.[1−3] It was previously demonstrated that HNA forms hightly selective and exceptionally stable duplexes with RNA[2,3] and that they are stable toward nuclease degradation.[2] From this point of view, HNA is superior to its DNA and RNA analogues as an antisense construct.[3] However, the HNA/RNA duplex is a poor substrate for RNase H,[3] and its antisense activity will most probably be due to a physical blockage of the targeted mRNA.[3] Hexitol nucleic acids are built up of phosphorylated 1,5-anhydro-D-*arabino*-2,3-dideoxyhexitol building blocks with a base moiety positioned in the 2-position. The conformational preference of the hexitol monomers are driven by the fact that the ring oxygen atom only contains unshared pairs (and thus a smaller substituent than a hydrogen atom) and that steric strains should be avoided in selecting the energetically most favorable conformation of a molecule (Westheimer model). As a result, the base moiety of the hexitol nucleosides are axially oriented.[4−6] When these monomers are polymerized, oligomers are obtained that form helical duplex structures as well with DNA and RNA and with itself (HNA), with a geometry resembling those of the Watson−Crick pairing natural nucleic acids.[2,3]

The formation of the helical structure is driven by stacking interactions between the bases, allowed by conformational changes in the phosphate backbone. This helical stabilization of the structure is not possible with equatorially oriented bases, as found in pyranose nucleic acids.[7,8] The six-membered hexitol ring can be considered as a mimic of a furanose ring, frozen in its 2′-exo,3′-endo conformation.[9−11] This is largely the conformation of the ribofuranose ring found in the A-form of dsRNA and dsDNA. It is not surprising, therefore, that initial CD studies demonstrate that HNA/DNA and HNA/RNA duplexes adopt a A-type conformation,[3] and this observation is now further investigated by NMR and X-ray studies. An intriguing observation is that the HNA/RNA duplex is more stable than an HNA/DNA duplex.[1−3] Dependent on the sequence studied, the latter duplex is sometimes of lower stability than a dsDNA hybrid.[3] The HNA/RNA duplex, however, is invariably more stable than all other associations of natural nucleic acids (dsDNA, dsRNA, DNA/RNA).[3] The order of duplex stability is given by HNA/HNA > HNA/RNA > HNA/DNA. The higher stability of duplexes with RNA as compared with DNA duplexes is generally explained by the propensity of the duplex to take an A-form-like structure. The present investigation describes a molecular dynamics study of HNA/RNA and HNA/DNA duplexes in an effort to try to explain the difference in stability between both complexes. This kind of study may lead to a better understanding of oligomeric complexes and, thus, to the design of more efficient RNA receptors.[11] The study itself was carried out on a HNA sequence (GCGTAGCG) containing all four natural bases.

† Present address: Janssen Research Foundation, Turnhoutseweg 30, B-2340 Beerse, Belgium.

(1) Van Aerschot, A.; Verheggen, I.; Hendrix, C.; Herdewijn, P. *Angew. Chem., Int. Ed. Engl.* **1995**, *34*, 1338−1339.

(2) Hendrix, C.; Verheggen, I.; Rosemeyer, H.; Seela, F.; Van Aerschot, A.; Herdewijn, P. *Chem. Eur. J.* **1997**, *3*, 110−120.

(3) Hendrix, C.; Rosemeyer, H.; De Bouvere, B.; Van Aerschot, A.; Seela, F.; Herdewijn, P. *Chem. Eur. J.* **1997**, *3*, 1513−1520.

(4) Verheggen, I.; Van Aerschot, A.; Toppet, D.; Snoeck, R.; Janssen, G.; Balzarini, J.; De Clercq, E.; Herdewijn, P. *J. Med. Chem.* **1993**, *36*, 2033−2040.

(5) Verheggen, I.; Van Aerschot, A.; Van Meervelt, L.; Rozenski, J.; Wiebe, L.; Snoeck, R.; Andrei, G.; Balzarini, J.; Claes, P.; De Clercq, E.; Herdewijn, P. *J. Med. Chem.* **1995**, *38*, 826−835.

(6) Declercq, R.; Herdewijn, P.; Van Meervelt, L. *Acta Crystallogr.* **1996**, *C52*, 1213−1215.

(7) Augustyns, K.; Van Aerschot, A.; Urbanke, C.; Herdewijn, P. *Bull. Soc. Chim. Belg.* **1992**, *101*, 119−130.

(8) Eschenmoser, A.; Dobler, M. *Helv. Chim. Acta* **1992**, *75*, 218−259.

(9) Herdewijn, P. *Liebigs Ann.* **1996**, 1337−1348.

(10) Maurinsh, Y.; Schraml, J.; De Winter, H.; Blaton, N.; Peeters, O.; Lescrinier, E.; Rozenski, J.; Van Aerschot, A.; De Clercq, E.; Busson, R.; Herdewijn, P. *J. Org. Chem.* **1997**, *62*, 2861−2871.

(11) Herdewijn, P. *Carbohydrate mimics: concepts and methods*; Chapleur, Y., Ed.; Verlag Chemie: Weinheim, Germany, 1998; pp 553−579.

S0002-7863(97)03721-9 CCC: $15.00 
Published on Web 05/19/1998

**Scheme 1.** Chemical Structure and Atom Numbering of the Anhydrohexitol Nucleosides Used in This Study[a]

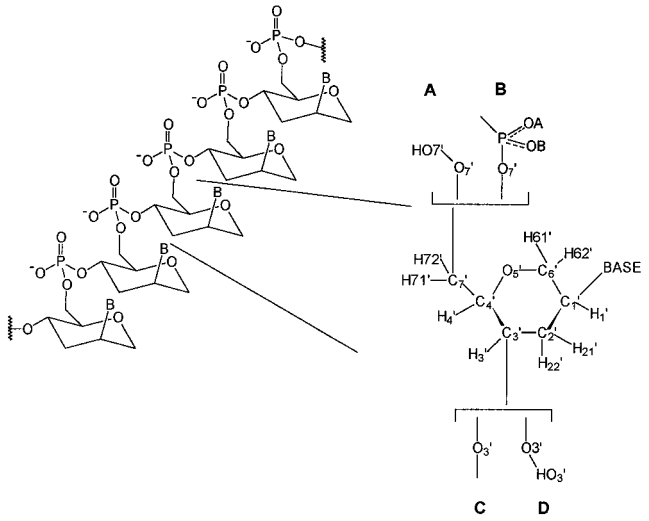


[a] The base moiety can be adenine, guanine, cytosine, or thymine.

## Methods

**Nomenclature.** The chemical structure and atom naming of anhydrohexitol nucleosides as used throughout the modeling and NMR experiments is given in Scheme 1. They are composed of a six-membered anhydrohexitol ring that is substituted at C1′ by one of the four different heterocycles attached by a C1′−N linkage. The heterocycles are the purine bases adenine (A) and guanine (G) and the pyrimidine bases cytosine (C) and thymine (T). In anhydrohexitol oligonucleotides (HNA), the individual anhydrohexitol residues are linked via 3′,7′-phosphodiester bonds. Such HNA oligonucleotides can form antiparallel duplexes with DNA or RNA oligonucleotides, and the general structure of the two hybrid complexes used in the present study are shown in Scheme 2.

## Synthesis

**1,5-Anhydro-6-*O*-monomethoxytrityl-2-(thymin-1-yl)-2,3-dideoxy-D-*arabino*-hexitol-4-yl-hydrogenphosphonate, Triethylammonium Salt (3a).** To 270 $\mu$L (3 mmol) of phosphorus trichloride in 30 mL of anhydrous $CH_2Cl_2$ cooled on an icebath was added 3.3 mL (30 mmol) of *N*-methylmorpholine and 690 mg (10 mmol) of 1,2,4-triazole. The mixture was stirred for 30 min at room temperature and subsequently cooled again, and 320 mg (0.6 mmol) of 1,5-anhydro-6-*O*-monomethoxytrityl-2-(thymin-1-yl)-2,3-dideoxy-D-*arabino*-hexitol (**1a**)[12] dissolved in 10 mL of $CH_2Cl_2$ was added dropwise over 15 min. The mixture was stirred for 10 min more at room temperature and poured into 25 mL of 1 M triethylammonium bicarbonate (TEAB) buffer. After separation of both layers, the aqueous phase was extracted once more with $CH_2Cl_2$, and the organics were dried and purified by flash chromatography on 20 g of silica gel (gradient of $CH_2Cl_2$−TEA 99:1 to $CH_2Cl_2$−TEA−MeOH 89:1:10). Product-containing fractions were washed once with 25 mL of 1 M TEAB buffer and dried, affording 344 mg (0.495 mmol, 82%) of the title product **3a** as a white foam. LSIMS (ThGly doped with NaOAc) *m*/*z* 659 (M + $3Na^+$, 1), 637 (M + $2Na^+$, 2), 273 ($MMTr^+$, 100). $^1$H NMR ($CDCl_3$): $\delta$ 1.27 (t, 9H, $J$ = 7 Hz, $CH_2CH_3$), 1.74 (s, 3H, $CH_3$), 1.94−2.11 (m, 1H, H-3′$_{ax}$), 2.61 (dm, 1H, H-3″$_{eq}$), 3.00 (q, 6H, $CH_2CH_3$), 3.34 (dd, 1H, $J$ = 4.5 and 10.4 Hz, H-5′), 3.45−3.60 (m, 2H, H-6′, H-6″), 3.79 (s, 3H, $OCH_3$), 3.89 (dd, 1H, $J$ = 3.4 and 13.4 Hz, H-1′$_{ax}$), 4.16 (d, 1H, $J$ = 13.6 Hz, H-1′$_{eq}$), 4.57 (m, 1H, H-4′), 4.73 (m, 1H, H-2′), 6.66 (d, 1H, $J$ = 625 Hz, P-H), 6.83 (d, $J$ = 8.7, 2H, aromatic H), 7.15−7.55 (m, 12H, aromatic H), 8.05 (s, 1H, H-6), 9.50 (br s, 1H, NH) ppm. $^{13}$C NMR ($CDCl_3$): $\delta$ 8.5 ($CH_2CH_3$), 12.7 ($CH_3$), 35.2 (C-3′), 45.3 ($CH_2CH_3$), 50.4 (C-2′), 55.1 ($OCH_3$), 62.7 (C-6′), 64.2 (C-4′, d, $J$ = 3.8 Hz), 68.4 (C-1′), 80.4 (C-5′, d, $J$ = 8 Hz), 86.2 ($Ph_3C$), 110.5 (C-5), 138.5 (C-6), 151.2 (C-2), 163.9 (C-4), 113.0, 126.8, 127.4, 127.7, 130.4, 135.5, 144.3, 158.4 (aromatic C) ppm.

**1,5-Anhydro-4-*O*-benzoyl-2-($N^6$-benzoyladenin-9-yl)-2,3-dideoxy-D-*arabino*-hexitol (2b).** An amount of 257 mg (0.4 mmol) of **1b**[12] was co-evaporated with pyridine and subsequently dissolved in 20 mL of anhydrous pyridine after which 110 $\mu$L (0.8 mmol) of benzoyl chloride was added. The mixture was stirred overnight at room temperature and quenched with 2 mL of methanol. After addition of some $NaHCO_3$, the mixture was concentrated and partitioned between $CH_2Cl_2$ and 5% of aqueous $NaHCO_3$. The organic phase was washed once more with 75 mL of aqueous $NaHCO_3$ and dried on $Na_2SO_4$. Evaporation left an oil that was co-evaporated with toluene. The foam was treated with 40 mL of 80% aqueous HOAc and left at RT for 1 h. Evaporation gave 400 mg of a light brown foam that was purified on silica gel with a methanol gradient in $CH_2Cl_2$ (100 to 96:4). The product-containing fractions were pooled affording 86 mg (0.18 mmol, 45%) of the title product **2b** as a white powder. LSIMS (ThGLy) *m*/*z* 474 ($MH^+$, 25), 240 ($BH_2^+$, 7). $^1$H NMR ($CDCl_3$): $\delta$ 2.21−2.39 (ddd, 1H, H-3′$_{ax}$), 2.84−2.98 (dm, $J$ = 13.5 Hz, 1H, H-3″$_{eq}$), 3.64−3.91 (m, 3H, H-5′, H-6′, H-6″), 4.13 (dd, 1H, $J$ = 2.6 and 13.1 Hz, H-1′$_{ax}$), 4.52 (dm, 1H, $J$ = 12.5 Hz, H-1′$_{eq}$), 5.07−5.14 (m, 1H, H-2′), 5.18−5.33 (m, 1H, H-4′), 7.35−7.65 (m, 6H, aromatic H), 7.91−8.08 (m, 4H, aromatic H), 8.70 (s, 1H) and 8.80 (s, 1H) (H-2, H-8), 9.63 (br s, 1H, NH) ppm. $^{13}$C NMR ($CDCl_3$): $\delta$ 33.1 (C-3′), 50.7 (C-2′), 61.4 (C-6′), 64.4 (C-4′), 69.1 (C-1′), 80.5 (C-5′), 123.2 (C-5), 142.0 (C-8), 149.6 (C-4), 151.7 (C-6), 152.5 (C-2), 164.8, 165.4 (2 × CO) ppm + aromatic signals.

**[1,5-Anhydro-2-(thymin-1-yl)-2,3-dideoxy-D-*arabino*-hexitol]-(4-6)-[1,5-anhydro-2-(adenin-9-yl)-2,3-dideoxy-D-*arabino*-hexitol]phosphate, Sodium Salt (5).** A portion of 86 mg (0.18 mmol) of **2b** and 145 mg (0.21 mmol) of the thymine hydrogenphosphonate **3a** were co-evaporated twice with anhydrous pyridine and dissolved in a 6 mL mixture of anhydrous pyridine and acetonitrile. One milliliter (0.5 mmol) of a dilution of pivaloyl chloride in pyridine was added, and the reaction mixture was stirred for 10 min at room temperature under a nitrogen atmosphere. Subsequently 2 mL of a 4% $I_2$ (w/v) solution in pyridine−water (96:4) was added, and stirring continued for another 10 min at room temperature. The mixture was diluted with 100 mL

**Scheme 2.** Schematic Drawing of the Two Hybrid Complexes Used in This Study[a]

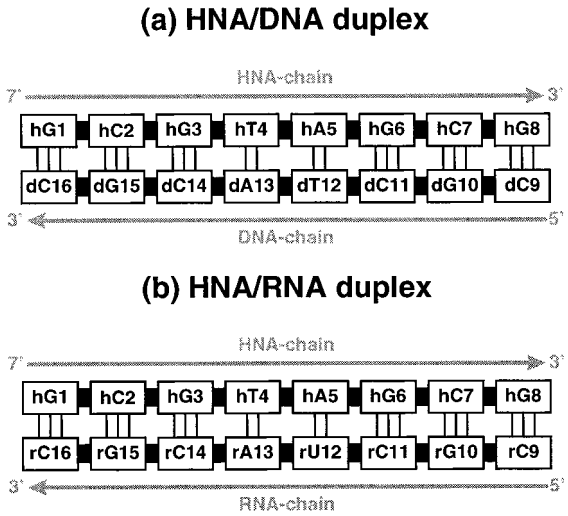


[a] The lowercase letter at the beginning of each residue name stands for the particular residue type: 'h' for anhydrohexitol, 'd' for deoxyribose, and 'r' for ribose. The residue numbering starts at the 7′-terminal side of the HNA chain and ends at the 3′-end of the DNA (HNA/DNA complex) or RNA strand (HNA/RNA complex). Residue 12 can be either thymidine (HNA/DNA duplex) or uridine (HNA/RNA duplex). The black boxes linking adjacent nucleotides indicate phosphodiester bridges, and hydrogen bonds between opposite residues are drawn by thin lines.

(12) De Bouvere, B.; Kerremans, L.; Rozenski, J.; Janssen, G.; Van Aerschot, A.; Claes, P.; Busson, R.; Herdewijn, P. *Liebigs Ann.* **1997**, 1453−1461.

**Scheme 3.** Synthesis of Hexitol Nucleic Acids TA Dimer Using Solution Phase H-Phosphonate Chemistry[a]

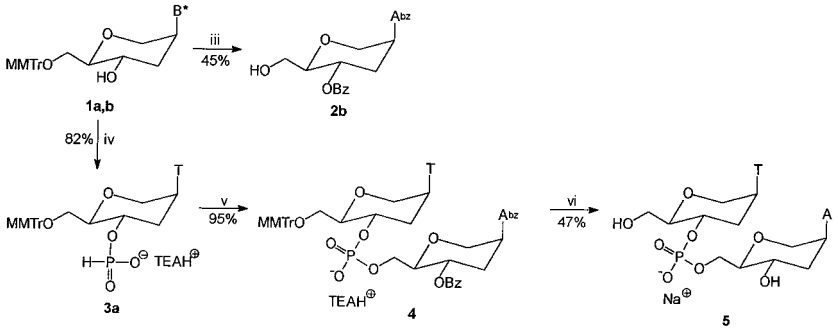


[a] **a**, B* = thymin-1-yl. **b**, B* = $N^6$-benzoyladen-9-yl. iii, benzoyl chloride, pyridine; 80% HOAc. iv, $PCl_3$, *N*-methylmorpholine, triazole, TEAB buffer. v, **3a** (1.15 equiv), **2b** pivaloyl chloride, pyridine−acetonitrile; iodine, TEAB buffer. vi, ammonia−ethanol; 80% HOAc; RP-HPLC; Dowex 50X8-200 ($Na^+$ form).

of $CH_2Cl_2$ and washed with 50 mL of 10% aqueous $Na_2S_2O_3$ and with 50 mL of 1 M TEAB. The organic phase was dried, evaporated, and purified by column chromatography on 20 g of silica gel (gradient of $CH_2Cl_2$−TEA 99:1 to $CH_2Cl_2$−TEA−MeOH 93:1:6) affording 200 mg (0.17 mmol, 95%) of the fully protected dimer. LSIMS (ThGly doped with NaOAc) *m*/*z* 1108 (M + $2Na^+$, 2) and 273 ($MMTr^+$, 100). The white foam obtained was dissolved in 20 mL of a 3:1 mixture of concentrated ammonia and ethanol and heated overnight at 40 °C. The mixture was evaporated and co-evaporated with 1,4-dioxane. The residue was dissolved in 20 mL of 80% aqueous acetic acid and heated at 60 °C for 1 h. After evaporation, the residue was partitioned between 10 mL of 0.1 M triethylammonium acetate (TEAA) solution and 10 mL of ether. The aqueous phase was washed 3 times more with 10 mL of diethyl ether and concentrated and purified by reverse phase HPLC on a polystyrene(divinyl benzene) support (PLRP-S, 250 × 9 mm) with an acetonitrile gradient in 0.1 M TEAA. Product-containing fractions were pooled, and the TEA salt was exchanged for the sodium salt by chromatography on a Dowex 50 × 8−200 cation-exchange resin under its sodium form. Lyophylization afforded 52 mg (85 $\mu$mol, 47% overall) as a white voluminous powder. LSIMS (ThGly) *m*/*z* 628 (M sodium salt + $Na^+$, 30), 606 (M sodium salt + $H^+$, 4).

**NMR Analysis of a HNA TA-Dimer.** A 7.5 mM solution of h(TA) was prepared in a 10 mM phosphate buffer (pH 7.0). The sample was lyophylized and redissolved twice in 99.996% $D_2O$. A Varian 500 Unity spectrometer with gradient indirect detection probe, operating at 499.6 MHz (1 H), and 33 °C was used. Data were processed on a SunSparc workstation with the standard VNMR software (version 5.1) and on a Silicon Graphics Indigo2 R10000 workstation (IRIX version 6.2) using the Felix95.0 software package (Biosym Technologies, San Diego). All proton spectra are internal referenced to the water signal at 4.64 ppm. The $^{31}P$ signal is external referenced to $H_3PO_4$ 85%. Gradient double quantum filtered phase sensitive cosy $^1H-^1H$ correlation spectra (GDQFCOPS[13]) consisted of 2048 pairs of real and imaginary points in $t_1$ and 4096 data points in $t_2$. To obtain maximum resolution, a reduced sweep width of 2000 Hz was used, covering only the anhydrohexitol signals. The data were apodized with a skewed sinebel squared function in both dimensions. The $^{31}P$ was decoupled on resonance and in the continuous mode. The NOESY[14] spectrum (mix = 300 ms) was performed with 512 pairs of real and imaginary points in $t_1$ and 2048 data points in $t_2$. To cover the full spectrum, a spectral width of 4800 Hz was used. Data were zero-filled in $t_1$ to 2048 and apodized with a skewed sinebel squared function in both dimensions.

**Computational Chemistry. Force Field Parameters and Partial Charges.** (i) RNA and DNA: Parameters and also the partial charges for the nucleoside bases, sugars, and phosphate moieties of the RNA and DNA strands were taken from the AMBER 4.1 force field parameter database.[15] (ii) HNA: Partial atomic charges of the HNA strand atoms were calculated using the RESP methodology,[16] involving a two-stage fit of the charges to the 6-31G*-derived electrostatic potential calculated using GAMESS.[17] The partial atomic charges of the HNA residues are shown in Scheme 4. The appropriate atom types for the HNA atoms were taken from the AMBER 4.1 parameter database and shown in Scheme 4. Force field parameters were also taken from AMBER 4.1 and used without modification. In the absence of experimental data regarding the relative stabilities and energy barriers between the different puckering forms of the anhydrohexitol rings, we could not thoroughly evaluate the assumption that the default AMBER parametrization performs properly for anhydrohexitol nucleosides as well. However, several test MD runs of more than 10 ns each on isolated anhydrohexitol nucleosides immersed in water boxes compared well with the average conformations derived from NMR experiments (data not shown). During these test calculations, the bases remained in axial orientation with respect to their anhydrohexitol moieties, and good agreement with the NMR conformations was found for the O7′−C7′−C4′−C3′ ($\gamma$) and C6′−C1′−N1−C2 ($\chi$) torsion angles (data not shown).

**Model Building.** (i) HNA/RNA complex: A model of d(GCGTAGCG)/r(CGCUACGC) in Arnott's canonical A-RNA geometry was used as the starting point. Using MidasPlus,[18] the p(GCGTAGCG) strand was subsequently docked onto the DNA strand of the DNA/RNA model.[19] The entire HNA strand was then energy minimized while its base atoms were template forced onto the corresponding positions of the DNA strand using a force constant of 10 kcal/mol·Å$^2$ on each base atom. Finally, the DNA strand was deleted, and the resulting HNA/RNA complex was energy minimized down to an rms energy gradient of 0.1 kcal/mol·Å by imposing a parabolic restraint on the base pair hydrogen bonds between 2.5 and 4.0 Å using a 10 kcal/mol·Å$^2$ force constant and a linear restraint at larger distances. This was followed by unrestrained minimization until the rms gradient dropped below 0.1 kcal/mol·Å. Care was taken to model each

(13) Davis, A. L.; Laue, E. D.; Keeler, J.; Moskou, D.; Loohman, J. *J. Magn. Reson.* **1991**, *94*, 637−644.

(14) States, D. J.; Haberkorn, R. A.; Ruben, D. J. *J. Magn. Reson.* **1982**, *48*, 286−292.

(15) Cornell, W. D.; Cieplak, P.; Bayly, C. I.; Gould, I. R.; Merz, K. M.; Ferguson, D. M.; Spellmeyer, D. C.; Fox, T.; Caldwell, J. W.; Kollman, P. A. *J. Am. Chem. Soc.* **1995**, *117*, 5179−5197.

(16) Bayly, C. I.; Cieplak, P.; Cornell, W. D.; Kollman, P. A. *J. Phys. Chem.* **1993**, *97*, 10269−10280.

(17) Schmidt, M. W.; Baldridge, K. K.; Boatz, J. A.; Elbert, S. T.; Gordon, G. S.; Jensen, J. H.; Koseki, S.; Matsunaga, N.; Nguyen, K. A.; Su, S.; Windus, T. L.; Dupuis, M.; Montgomery, J. A. *J. Comput. Chem.* **1993**, *14*, 1347−1363.

(18) Ferrin, T. E.; Huang, C. C.; Jarvis, L. E.; Langridge, R. *J. Mol. Graphics* **1988**, *6*, 13−27.

(19) We also experimented to model the HNA/RNA duplex in a B-like geometry but were unsuccessful to obtain starting structures with reasonable backbone torsion angles along the HNA strand. Comparison of the conformation of the HNA six-membered sugar ring with each of the two possible low-energy conformations of a five-membered deoxyribose sugar ring (C2′- and C3′-*endo*) indicates that the HNA sugar resembles the C3′-*endo* conformation much better than the C2′-*endo* puckered form (data not shown). In fact, after superimposition of the corresponding nucleoside base atoms, a rms deviation between the sugar−phosphate backbone atoms (O5′−C5′−C4′−C3′−O3′ for the deoxyribose sugar versus O7′−C7′−C4′−C3′−O3′ for the HNA sugar) of <1 Å was calculated when the deoxyribose was modeled as C3′-*endo* and >3 Å for the deoxyribose in a C2′-*endo* conformation.

**Scheme 4.** Force Field Atom Types and Partial Charges of the Four Different Anhydrohexitol Nucleotides Used in This Study

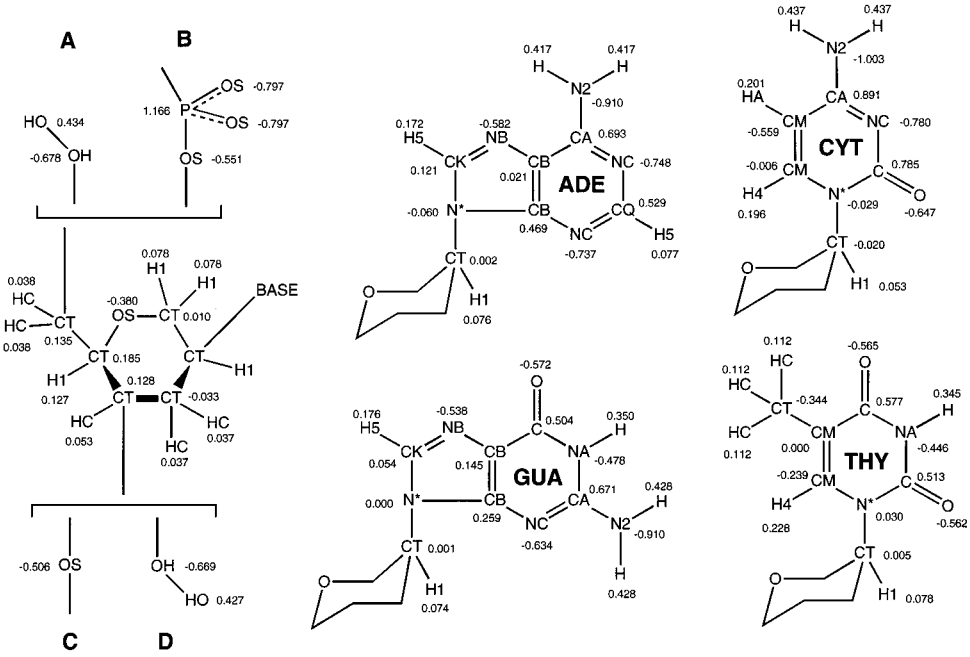


anhydrohexitol ring in a chair-like conformation with the base moieties oriented axially, but during minimization it was found that the hG1 anhydrohexitol ring had flipped from a chair- to a twistboat-like conformation, while keeping the guanine base in an axial orientation.

The resulting duplex was soaked in a rectangular box of TIP3P waters that extended approximately 12 Å in each direction from the nucleic acid atoms. This seems to be adequate to reproduce the global structure and dynamics in solution.[20] Fourteen water molecules whose oxygens were located at positions of highest negative electrostatic potential were replaced by sodium ions. This yielded a total of 3752 waters. (ii) The HNA/DNA complex was prepared from the minimized coordinates of the HNA/RNA system after deletion fo the 2′-hydroxyl groups of the ribose sugars and proper adjustment of partial charges and atom types. After minimization, the whole system was submerged in a rectangular box of waters. Sodium counterions were added in a similar fashion as for the HNA/RNA complex. In total, 3781 TIP3P waters were included in the HNA/DNA simulation. The initial box size was ∼58 by ∼50 by ∼47 Å$^3$ for both simulations.

**Molecular Dynamics.** Periodic boundary conditions were applied using constant temperature (300 K) and constant pressure (1 bar) conditions. Berendsen temperature coupling was used with separate but equal heat bath coupling time constants of 0.4 ps$^{-1}$ for solute and solvent atoms.[21] The compressibility of the systems was set to 44.6 × 10$^{-6}$ bar$^{-1}$, and the pressure relaxation time was defined at 0.4 ps$^{-1}$.[21] Simulations were run with SHAKE on all bond lengths,[22] a 2 fs time step, a 9 Å cutoff for Lennard−Jones interactions, and the nonbonded pairlist updated every 10 steps. Calculations were performed with the SANDER module of AMBER 4.1.[15] The results were analyzed with the CARNAL module. No restraints were applied during the production runs. The particle mesh Ewald (PME) method was used for the treatment of long-range electrostatic interactions.[23] The PME charge grid spacing for both simulations was approximately 1.0 Å in each direction. The order of the $\beta$-spline interpolation was 4, and the direct sum tolerance was set to 10$^{-6}$. The systems were minimized until the rms energy gradient dropped below 0.1 kcal/mol·Å. Subsequently, the systems were heated to 300 K over 10 ps, after which time production runs were initiated. The simulations were continued for 1.1 ns each, and conformations were saved every 50 fs. Final box dimensions were ∼56 by ∼48 by ∼45 Å$^3$ for both simulations. Only the final 1 ns were used for analysis, except where noted otherwise.

**Spatially Resolved Solvent Densities.** Spatially resolved solvent densities were calculated on the final 0.5 ns of each trajectory. Rotations and translations of the complexes within their boxes were removed from the trajectories by using the average structure of each double helix to establish a solute-fixed coordinate frame. Solvent densities were calculated by determining water oxygen positions from rms coordinate fit frames in 0.5 × 0.5 × 0.5 Å$^3$ grid volumes. The value of each grid volume represents the number of times a water oxygen atom was found within the 0.125 Å$^3$ of that particular grid volume. For 10 000 frames (the final 500 ps of each simulation), the expected number of water oxygens per grid volume, assuming bulk water density, is 41.6. The value at each grid volume was then converted to a density relative to the expected bulk water density. As an example, 83.2 and 124.8 hits per 0.125 Å$^3$ volume element are equal to 2 and 3 times the expected bulk water density. These grid values were then contoured in a manner analogous to the contouring of electron density in crystallographic diffraction studies. Results were visualized using Quanta (Biosym/MSI, San Diego).

**Solvent Accessible Surface Areas.** The solvent accessible surface area (SASA) of the double helices were calculated at each dynamics frame using the 'dms' module of the MidasPlus suite of programs.[18] A solvent probe radius of 1.4 Å and van der Waals radii of 1.9, 1.4, 1.5, and 1.9 Å for C, O, N, and P, respectively, were used.

## Results

**Chemical Synthesis of the HNA TA Dimer.** The chemical synthesis of the protected hexitol nucleoside monomers has been described before.[12] Assembly of the monomers into the h(TA) dimer was done according to standard H-phosphonate chemistry and was carried out in solution as described in Scheme 3. The tritylated anhydrohexitol nucleoside analogue **1a** was converted to the triethylammonium hydrogen phosphonate salt **3a** in 82% yield using phosphorus trichloride.[24] The adenine counterpart **1b** was reacted with benzoyl chloride, and the obtained crude was treated with 80% aqueous acetic acid for 1 h at RT. Silica

(20) Norberto de Souza, O.; Ornstein, R. L. *Biophys. J.* **1997**, *72*, 2395−2397.

(21) Berendsen, H. J. C.; Postma, J. P. M.; van Gunsteren, W. F.; DiNola, A.; Haak, J. R. *J. Chem. Phys.* **1984**, *81*, 3684−3690.

(22) van Gunsteren, W. F.; Berendsen, H. J. C. *Mol. Phys.* **1977**, *34*, 1311−1327.

(23) Essmann, U.; Perera, L.; Berkowitz, M. L.; Darden, T.; Lee, H.; Pedersen, L. G. *J. Chem. Phys.* **1995**, *103*, 8577−8593.

(24) Froehler, B. C.; Ng, P. G.; Matteucci, M. D. *Nucleic Aicds Res.* **1986**, *14*, 5399−5407.

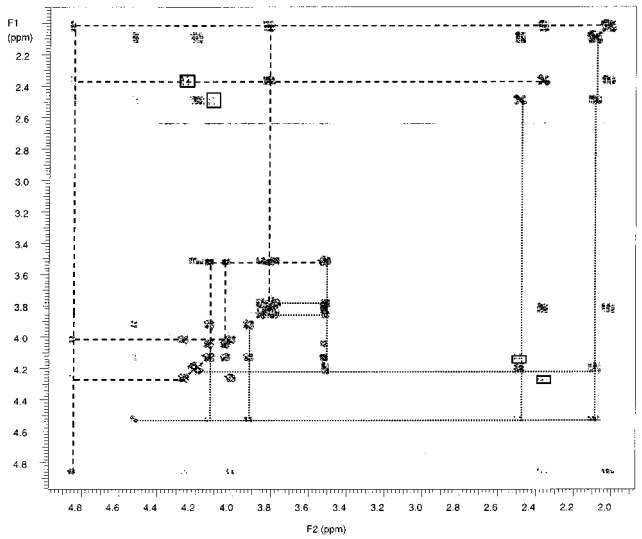


**Figure 1.** Overview of the non-$^{31}$P decoupled [$^1$H,$^1$H]GDQFCOPS spectrum. The hT1 signals are connected with dotted lines; the hA2 signals are connected with dashed lines. The long-range H61′-H21′ cross-peaks are marked in boxes.

**Table 1.** Measured in $D_2O$ at 33 °C, Internal Referenced to the Water Signal (4.64 ppm)[a]

| Section A: List of Chemical Shifts[a] | | | Section B: Coupling Constants in Hz[b] | | |
|---|---|---|---|---|---|
| | chemical shifts | | | $J_{H-H}$ | |
| | hT1 | hA2 | **1b** | hT1 | hA2 |
| H1′ | 4.52 | 4.88 | 1′−21′ | 2.5 | 2.6 |
| H21′ | 2.48 | 2.36 | 1′−22′ | 2.5 | 2.9 |
| H22′ | 2.09 | 2.02 | 1′−61′ | 2.0 | 2.0 |
| H3′ | 4.20 | 3.82 | 1′−62′ | 2.9 | 2.0 |
| H4′ | 3.51 | 3.54 | 21′−61′ | 2.0 | 2.0 |
| H61′ | 4.13 | 4.26 | 21′−22′ | 13.7 | 13.7 |
| H62′ | 3.92 | 4.01 | 21′−3′ | 5.0 | 4.9 |
| H71′ | 3.86 | 4.13 | 22′−3′ | 10.7 | 11.7 |
| H72′ | 3.78 | 4.04 | 3′−4′ | 8.8 | 9.8 |
| H6/H8 | 7.74 | 8.32 | 4′−71′ | 2.9 | 2.9 |
| H2 | | 8.18 | 4′−72′ | 5.9 | 1.9 |
| $CH_3$ | 1.77 | | 61′−62′ | 13.7 | 12.7 |
| P | 0.88 | | 71′−72′ | 12.7 | 11.7 |

[a] The phosphorus signal is referenced to $H_3PO_4$ (85%). [b] Estimated in a $^{31}$P-decoupled GDQFCOPS spectrum, using first-order analysis.

gel purification afforded 45% of the 4′-protected building block **2b**. Under activation by pivaloyl chloride **3a** (1.15 equiv) was reacted with **2b** for 10 min at RT, followed by the addition of an aqueous pyridine solution of iodine and further stirring for 10 min at RT. The described phosphate diester **4** was isolated as the triethylammonium salt by silica gel chromatography in 95% yield. Following deprotection (28% aqueous ammonia−EtOH 3:1, 15 h, 40 °C; 80% aqueous HOAc, 1 h, 60 °C), the dimer **5** was purified by RP HPLC and converted to its sodium salt in 47% overall yield.

**NMR Analysis Confirms the Axial Orientation of Base Moieties in an h(TA) Dimer.** The conformation of the individual hexitol nucleosides in a dimer was studied on an TA sequence. The resonance assignment in h(TA) was done with a [$^1$H,$^1$H]GDQFCOPS spectrum (Figure 1). The $J_{H-P}$ in the pattern of the signals hT1:3′, hT1:21′ (long range), hA2:4′ (long range), hA2:h71′, and hA2:72′ arise from the 3′ to 7′ fosfodiester linkage between hT1 and hA2.[25] A $^{31}$P decoupled [$^1$H,$^1$H]-GDQFCOPS spectrum was used to determine the coupling

(25) Blommers, M. J. J.; Nanz, D.; Zerbe, O. *J. Biomol. NMR* **1994**, *4*, 595−601.

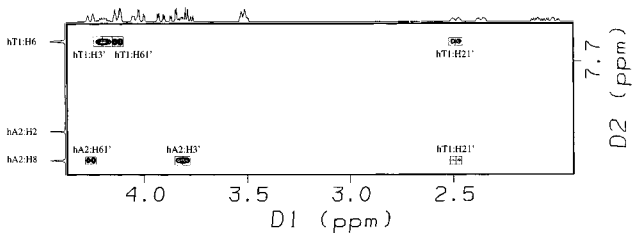


**Figure 2.** Expansion of the NOESY spectrum showing the interactions of the hT1:H6 and hA2:H8 protons with the anhydrohexitol moieties. Observed intraresidue NOE cross-peaks correspond to an anhydrohexitol conformation depicted in Scheme 5. The interresidue cross-peak of hA2:H8 → hT1:H21′ is marked in gray.

**Scheme 5.** Idealized Conformation of the HA Unity[a]

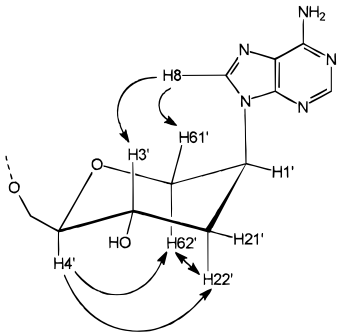


[a] Observed intraresidue NOE interactions which confirm the chair conformation of the anhydrohexitol unit are indicated by arrows.

constants listed in Table 1, SectionB. The large coupling constants $J_{H22'-H3'}$ and $J_{H3'-H4'}$ (8−11 Hz) indicate an axial position of the involved protons where the dihedral angles are close to 180°, while the small couplings in the pattern of the H1′ (2−3 Hz) suggest an equatorial position of the involved proton. These data correspond with an anhydrohexitol in a chair conformation with the base substituent in an axial position.[4−6] The "W" conformation of the atoms H61′−C6′−C1′−C2′−H21′ in this chair is confirmed by the long-range coupling $J_{H61'-H21'}$ in both hexitol rings (Figure 1). This result is according to what is described on the individual hA monomer.[4] A NOESY spectrum of h(TA) showed cross-peaks of hT1:H6 and hA2:H8 base protons with H3′, H21′ (only in hT1), and H61′ of their anhydrohexitols respectively (Figure 2). Between H4′, H22′ and H61′ were also neocontacts observed (data not shown). The occurrence of these NOE interactions is in agreement with the assignment of the anhydrohexitol conformation, which was based on values of coupling constants (Scheme 5). This NOE cross-peak pattern also indicates that the bases are in an anti position ($\chi = -120 \pm 60°$) where the H8/H6 of adenine and thymine, respectively, are located above the anhydrohexitol ring. These data support the selection of the starting conformation (i.e., HNA with axially positioned base moiety) for the modeling experiment.

**Geometric Features and Flexibility of the HNA/RNA and HNA/DNA Helices. Rms Deviation.** A stereo figure of the average structures of HNA/DNA and HNA/RNA is shown in Figure 3. Over the course of the entire simulation, the HNA/RNA complex remains close to its starting A-DNA-like geometry with an average rms deviation 1.4 Å from the start conformation (Figure 4a). The average minor groove width calculated for this complex, 13 Å, is closer to the 11 Å of A-type DNA than it is to the 6 Å of B-DNA (Figure 4b). In the case of the HNA/DNA duplex, however, the structure remains close to an A-DNA form for the first 300 ps but then deviates on the average more than 2.0 Å from the A-DNA-like starting

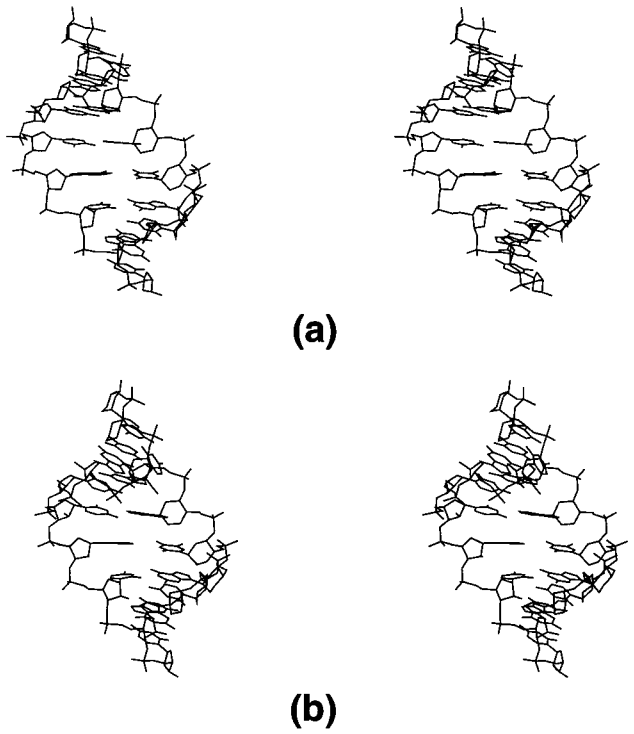


**Figure 3.** Stereo figure of the average structure of HNA/DNA (a) and HNA/RNA (b).

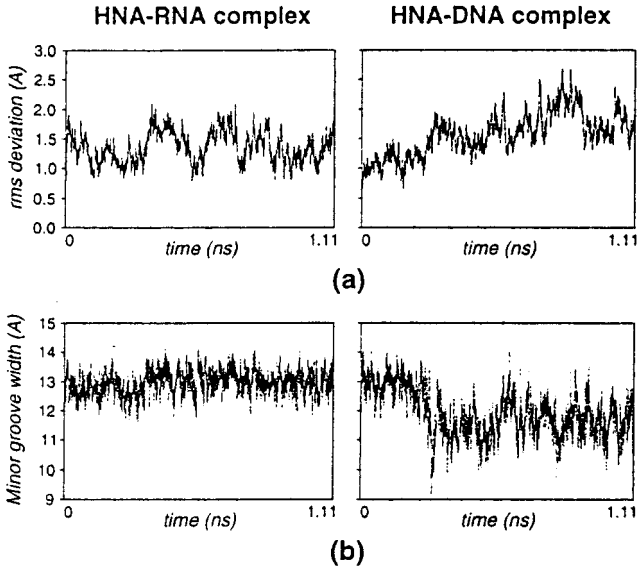


**Figure 4.** (a) Variation of the rms deviation from the start conformation as a function of time for the HNA/RNA complex (left) and HNA/DNA complex (right). (b) Variation of the minor groove width as a function of time for the HNA/RNA complex (left) and HNA/DNA complex (right). Minor groove widths were calculated by taking the perpendicular separation of helix strands drawn through phosphate groups, diminished by 5.8 Å to account for van der Waals radii of phosphate groups.

conformation during the second half of the simulation. This increase in rms deviation is accompanied by a decrease in minor groove width from 13 to less than 12 Å (Figure 4b).

**Anhydrohexitol Puckering.** Puckering parameters and standard deviations calculated for the six-membered anhydrohexitol rings (HNA strands) in the HNA/RNA and HNA/DNA double helices are given at the end of Table 2. The average value and standard deviation of the phase angles $\theta$ and $\varphi$, calculated over all of the eight anhydrohexitol residues, is 29.5(51.3) and 155.0(105.6)° for the anhydrohexitol residues in the HNA/RNA helix and 26.0(43.2) and 133.9(99.1)° for the HNA/RNA double helix. These average values are indicative of a chair conformation, although significantly flattened and tending toward a boat conformation. However, if the terminal anhydrohexitol residues (hG1 and hG8) are excluded from the calculations, then the average value of the $\theta$ and $\varphi$ phase angles are 10.3(5.4) ($\theta$) and 142.0(102.5)° ($\varphi$) and 10.6(5.4) ($\theta$) and 134.8(98.8)° ($\varphi$) for the HNA/RNA and HNA/DNA double helices, respectively. These values are typical for a slightly flattened chair conformation, with the large standard deviations of the $\varphi$ angles being indicative of small deviations from the chair conformation toward boat- and twist boat-like conformations with almost equal probability of occurrence.

Figure 5 shows the time course and polarplots of the $\theta$ and $\varphi$ pucker phase angles of residues hG1 and hT4 in the HNA/RNA and HNA/DNA double helices. The phase angles of hG1 in the HNA/RNA and HNA/DNA duplexes are shown in Figure 5, panels a and b, respectively, while hT4 is represented in Figure 5, panels c (HNA/RNA) and d (HNA/DNA). The puckering phase angles of residues hC2−hG8 are very similar to the values calculated for residue hT4; hence, hT4 was taken as a representative in this figure for the rest of the residues. From the data in Figure 5, it is clear that the anhydrohexitol ring of hT4 (and thus also residues hC2−hG8) in both the HNA/RNA and HNA/DNA duplexes remains close to a chair-like conformation ($\theta \sim 0°$; $\varphi \sim$ indefinite) throughout the simulation, with the base moiety oriented axially onto the anhydrohexitol ring. This is not entirely surprising as this conformation was taken as the starting conformation for residues hC2−hG8. On the other hand, in both the HNA/RNA and HNA/DNA duplexes, the anhydrohexitol ring of residue hG1 was initially placed in a boat-like conformation, and this was found to have significant consequences on the puckering behavior of this residue during the two MD simulations. In the HNA/RNA simulation (Figure 5a), hG1 undergoes already after a few picoseconds a quick transition from boat ($\theta \sim 90°$; $\varphi \sim 360°$) to inverted chair, in which the guanine base gets reoriented from axial to equatorial ($\theta \sim 180°$; $\varphi \sim$ indefinite). Also, a similar transition takes place in the HNA/DNA simulation (Figure 5b), but here the initial boat conformation ($\theta \sim 90°$; $\varphi \sim 0°$) remains for ∼0.6 ns before converting to inverted chair.

**Ribose and Deoxyribose Puckering.** The ribose sugars of the RNA strand in the HNA/RNA duplex remain close to a C3′-*endo* conformation ($P \sim 18°$), which is typical for the canonical A-family, while the deoxyribose sugar puckering of the HNA/DNA duplex interchanges between C2′-*endo* ($P \sim 162°$) and C3′-*endo*, giving an average puckering phase angle of ∼90° (Table 2). The time course and polarplots of the individual sugar pucker phase angles of the DNA and RNA strands in both duplexes are shown in Figure 6. The RNA strand in the HNA/RNA heteroduplex is represented in Figure 6a for each nucleotide going from the 5′- (rC9) to the 3′-end (rC16). The corresponding DNA strand in the HNA/DNA complex is shown alongside in Figure 6b. From the data in Figure 6a, it is obvious that the RNA strand is clearly not repuckering on a nanosecond time frame, except for the few repuckering events of the terminal rC16. However, it is likely that this latter event represents an artifact of the simulation, as rC16 is base-paired to hG1, which is repuckering from a boat to an inverted chair conformation after a few picoseconds in the simulation (see above). As this repuckering reorients the guanine base from an axial to an equatorial orientation, it is therefore likely that the observed repuckering of the rC16 ribose sugar is a direct consequence of its interaction with hG1.

**Table 2.** Torsion Angles and Puckering Parameters with Standard Deviations in Parentheses Averaged over All the Residues[a]

| | HNA/RNA duplex | | HNA/DNA duplex | | | | |
|---|---|---|---|---|---|---|---|
| | HNA strand | RNA strand | HNA strand | DNA strand | A-RNA[b] | A-DNA[b] | B-DNA[b] |
| α (deg)[c] | 266.6 (54.4) | 280.1 (10.8) | 255.1 (71.5) | 283.7 (11.0) | 292 | 310 | 314 |
| | 281.9 (9.1) | 280.2 (10.2) | 283.1 (8.9) | 284.2 (10.4) | | | |
| $\beta$ (deg)[c] | 183.0 (54.5) | 176.0 (10.5) | 173.9 (23.8) | 175.3 (10.5) | 178 | 172 | 213 |
| | 166.7 (8.6) | 174.7 (10.2) | 164.5 (8.4) | 173.7 (9.7) | | | |
| $\gamma$ (deg)[c] | 83.4 (43.8) | 65.5 (10.4) | 88.9 (48.6) | 67.7 (32.0) | 54 | 41 | 36 |
| | 80.8 (38.5) | 65.9 (9.5) | 84.5 (43.2) | 60.4 (10.6) | | | |
| $\delta$ (deg)[c] | 81.0 (27.9) | 83.8 (18.5) | 81.8 (26.2) | 107.0 (23.8) | 82 | 79 | 157 |
| | 71.0 (7.1) | 78.4 (6.5) | 72.6 (6.6) | 102.9 (22.7) | | | |
| $\epsilon$ (deg)[c] | 219.9 (23.9) | 202.6 (11.2) | 215.3 (22.6) | 191.6 (10.1) | 207 | 214 | 155 |
| | 211.5 (11.0) | 203.3 (10.6) | 208.6 (10.9) | 191.8 (9.8) | | | |
| $\zeta$ (deg)[c] | 276.1 (42.2) | 289.4 (9.1) | 278.5 31.5) | 277.6 (13.0) | 289 | 282 | 264 |
| $\chi$ (deg)[c] | 243.3 (22.0) | 210.7 (13.7) | 241.1 (18.5) | 229.2 (20.7) | 202 | 206 | 262 |
| | 235.4 (13.6) | 208.6 (13.1) | 237.0 (14.0) | 229.6 (22.1) | | | |
| pucker amplitude (Å)[d] | 0.520 (0.041) | 0.381 (0.058) | 0.525 (0.055) | 0.371 (0.061) | | | |
| | 0.517 (0.041) | 0.387 (0.054) | 0.513 (0.040) | 0.373 (0.059) | | | |
| pucker phase angle $\theta$ (deg)[d] | 29.5 (51.3) | | 26.0 (43.2) | | | | |
| | 10.3 (5.4) | | 10.6 (5.4) | | | | |
| pucker phase angle g (deg)[d] | 155.0 (105.6) | | 133.9 (99.1) | | | | |
| | 142.0 (102.5) | | 134.8 (98.8) | | | | |
| pucker phase angle *P* (deg)[e] | | 31.1 (43.0) | | 97.5 (55.5) | C3′-endo | C3′-endo | C2′-endo |
| | | 17.3 (11.5) | | 90.7 (53.8) | | | |

[a] First value in each entry or with the Four Terminal Residues (hG1, hG8, d/rC9, d/rC16) excluded from the calculations (second value in each entry). The various duplex structures are specified. The average values were calculated by determining the values for each dynamic frame during the final last nanoseconds of the simulation followed by averaging. The values in parentheses represent the standard deviation of this average. [b]Data for these duplexes were taken from Saenger.[30] [c]Torsion angles defined by O3′−P−O7′−C7′ (α), P−O7′−C7′−C4′ ($\beta$), O7′−C7′−C4′−C3′ ($\gamma$), C7′−C4′−C3′−O3′ ($\delta$), C4′−C3′−O3′−P ($\epsilon$), C3′−O3′−P−O7′ ($\zeta$), C6′−C1′−N1−C2 ($\chi$). [d]Calculated according to Cremer and Pople.[32] [e]Calculated according to Altona and Sundaralingam.[34]

On the other hand, from the data in Figure 6b, it is clear that the DNA strand is repuckering between C2′-*endo* and C3′-*endo* throughout the entire simulation. The time course of the transition from C3′-*endo* to C2′-*endo* pucker is also evident from this figure. All of the DNA sugars have repuckered within <300 ps.

**Backbone Torsion Angles.** The data in Table 2 show that the HNA/RNA and HNA/DNA helices are characteristic of the canonical A-family of oligonucleotide structures. The $\gamma$ torsion angles of the HNA strands in the two hybrid duplexes show large standard deviations, and this is caused by the large deviations of this angle in the residues along the 6′-end of the HNA strands, i.e., hG1 and hC2. While the average value of $\gamma$ of residues hG3−hG8 centers around ∼65°, the average value of $\gamma$ at hC2 is ∼170° in both duplexes. In the case of hG1, a transition in $\gamma$ (going from ∼60° to ∼180°) is observed in both complexes after ∼0.6 ns (data not shown). In the HNA/DNA simulation, this transition is accompanied by a simultaneous repuckering of the hG1 anhydrohexitol ring from boat to inverted chair (see above and also Figure 5b), while in the case of the HNA/RNA simulation, this transition is accompanied by a relaxation of the $\varphi$ puckering phase angle (Figure 5a).

Interestingly, the RNA strand of the HNA/RNA duplex is less flexible than the DNA strand of the HNA/DNA duplex, as judged by looking at the standard deviations in backbone angles presented in Table 2. Especially $\delta$, $\zeta$, and $\chi$ show enhanced fluctuation in the DNA strand as compared to the corresponding values in the RNA chain. This is in agreement with the increased flexibility of the deoxyribose sugar ring of the DNA strand as compared to the more rigid ribose puckering observed for the RNA chain (Table 2 and Figure 6).

**Base Pair Hydrogen Bonds.** A summary of the hydrogen bond lengths and their standard deviations between the base pairs in each of the two complexes is given in Table 3. It is clear from this table that there are no fundamental differences in hydrogen bonding properties of the HNA/DNA and HNA/RNA complexes. The corresponding base pairs in the two complexes remain strongly hydrogen bonded throughout the entire simulation, and the individual hydrogen bond distances and standard deviations for HNA/DNA and HNA/RNA are very similar. The only significant differences are found along the termini of the helices, where larger standard deviations are observed in the case of the HNA/DNA complex as compared to HNA/RNA.

**Solvation of the HNA/RNA and HNA/RNA Double Helices. Solvent accessible surface area.** A decomposition of the total solvent accessible surface area (SASA) in polar and hydrophobic components is tabulated in Table 4. To do this, the area formed by N, O, and P atoms was defined as polar, whereas the area defined by C atoms was taken as being hydrophobic. Hydrogen atoms were not included in the surface area calculations. The total SASA is approximately identical for the HNA/RNA and HNA/DNA complexes and fluctuates around 2440 Å$^2$. Nevertheless, the SASA of the HNA/RNA complex is significantly more polar than that of the HNA/DNA complex. This difference is mainly due to the ribose moiety of the RNA strand whose SASA is more polar than the corresponding area of the deoxyribose moiety of the DNA strand. When the contributions of the 2′-OH groups to the SASA are ignored by assuming a van der Waals radius of 0 Å for these oxygens, the polar and hydrophobic fractions of the total SASA become almost identical for the two complexes (Table 4).

In Figure 7, the SASA of each of the two averaged structures is color-coded according to the type of its underlying atom: N, blue; O, red; P, purple; and C, gray. A view into the minor groove of HNA/RNA and HNA/DNA is shown in Figure 7, panels a and b, respectively, while the corresponding major grooves are shown in Figure 7, panels c and d. Inspection of these latter two panels shows that the major grooves of HNA/RNA and HNA/DNA are virtual identical in terms of hydrophobic/hydrophilic character when comparing the relative amount of blue, red, and gray coloring. Hence, it can be expected that the solvation pattern of each of these two major

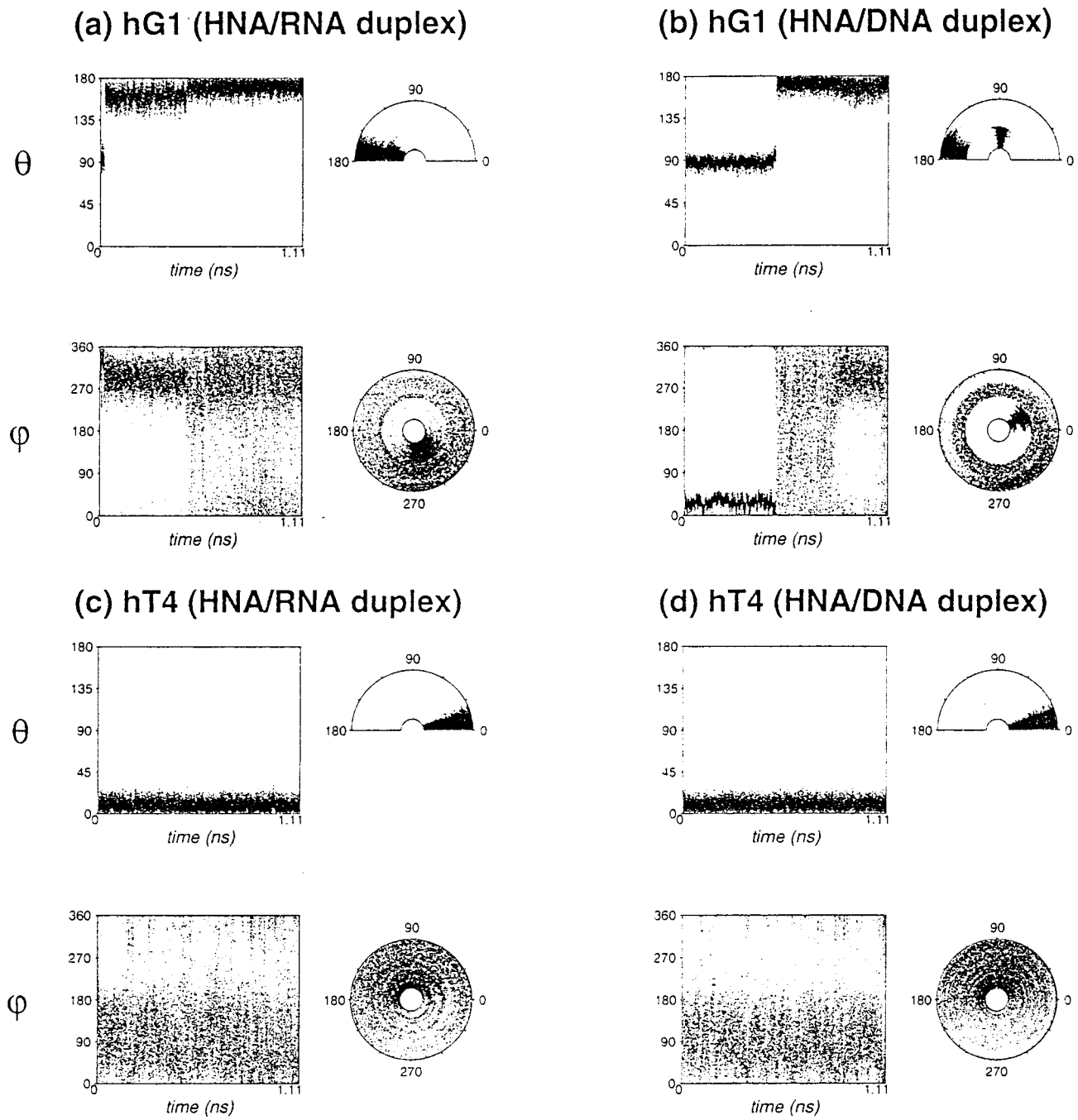


**Figure 5.** Sugar pucker $\theta$ and $\varphi$ phase angles of residues hG1 and hT4 in the HNA/RNA and HNA/DNA double helices. The $\theta$ and $\varphi$ phase angles of hG1 in the HNA/RNA and HNA/DNA duplexes are shown in panels a and b, respectively, while hT4 is represented in panels c (HNA/RNA) and d (HNA/DNA). The left side of each plot depicts a phase angle versus time graph, and the right side shows a polarplot of the phase angle. Time increases when going from the inner circle of the polarplot (0 ns) toward its circumference (1.11 ns).

grooves will be highly comparable to each other. On the other hand, however, the 2′-OH group of the RNA strand, which is flanking the minor groove of the HNA/RNA duplex, but which is not present in the HNA/DNA complex, is responsible for the enhanced red coloring of the HNA/RNA SASA (Figure 7a) as compared to the surface of HNA/DNA (Figure 7b). It is therefore likely that substantial differences in hydration patterns between the two duplexes can be expected along the minor groove sides of the two double helices and that the 2′-OH group of the RNA strand should play an important contribution in this.

**Spatially Resolved Solvent Densities.** Analysis of the spatial distribution of the water oxygen atoms around each double helix was carried out to further investigate possible differences in hydration between the HNA/DNA and HNA/RNA complexes. Hydration patterns around the phosphate moieties and in both the minor and major grooves were investigated.

**(1) Phosphate Groups.** Very little preferential hydration of the phosphate groups is visible. There is no occurrence of single water molecules simultaneously hydrogen bonding to each of the free oxygen atoms of the phosphates, which is in agreement with the A-DNA crystal structure of d($^{I}$CGCG)[26] and with the calculations on A-RNA by Cheatman and Kollman,[27] but in disagreement with theoretical calculations done by Clementi and

(26) Conner, B. N.; Takano, T.; Tanaka, S.; Itakura, K.; Dickerson, R. E. *Nature* **1982**, *295*, 294−299.

(27) Cheatham, T. E., III; Kollman, P. A. *J. Am. Chem. Soc.* **1997**, *119*, 4805−4825.

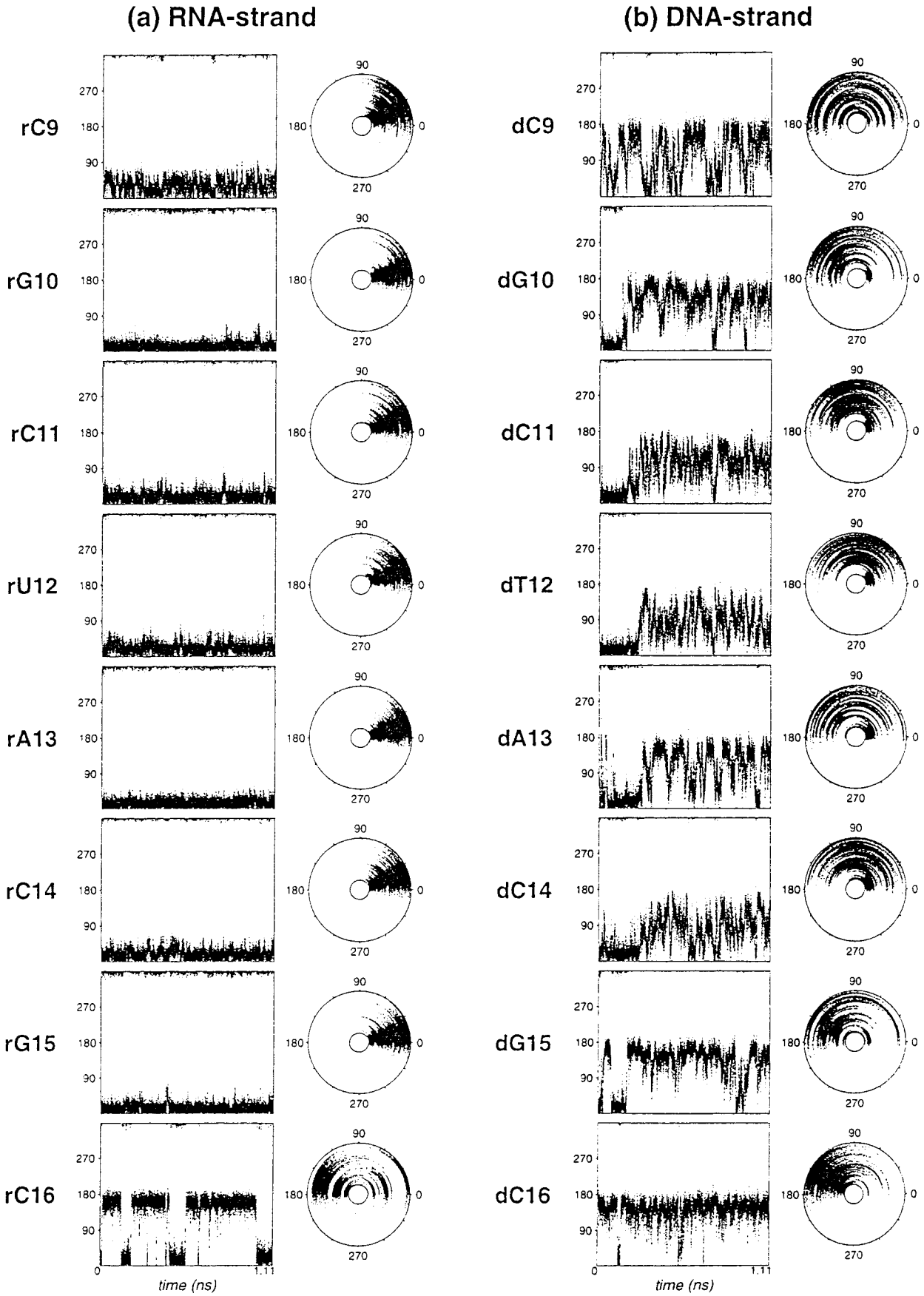


**Figure 6.** Time course and polarplots of the puckering phase angle *P* of (a) the ribose rings of the RNA strand in the HNA/RNA complex and (b) the deoxyribose rings of the DNA strand in the HNA/DNA complex. Time increases when going from the inner circle of each polarplot (0 ns) toward its circumference (1.11 ns).

**Table 3.** Average Hydrogen Bond Lengths (and Standard Deviations) between Interstrand Base Pairs Calculated over the Last 500 ps of Each Simulation[a]

| HNA/RNA | | HNA/DNA | |
|---|---|---|---|
| (hG1)H2B···(rC16)O2 | 1.93(0.14) | (hG1)H2B···(dC16)O2 | 1.97(0.22) |
| (hG1)H1···(rC16)N3 | 1.98(0.10) | (hG1)H1···(dC16)N3 | 2.01(0.16) |
| (hG1)O6···(rC16)H42 | 2.01(0.19) | (hG1)O6···(dC16)H42 | 2.17(0.56) |
| (hC2)O2···(rG15)H21 | 1.87(0.11) | (hC2)O2···(dG15)H21 | 1.89(0.12) |
| (hC2)N3···(rG15)H1 | 1.93(0.09) | (hC2)N3···(dG15)H1 | 1.95(0.09) |
| (hC2)H4A···(rG15)O6 | 1.99(0.17) | (hC2)H4A···(dG15)O6 | 1.99(0.17) |
| (hG3)H2B···(rC14)O2 | 1.86(0.11) | (hG3)H2B···(dC14)O2 | 1.88(0.12) |
| (hG3)H1···(rC14)N3 | 1.96(0.10) | (hG3)H1···(dC14)N3 | 1.96(0.10) |
| (hG3)O6···(rC14)H42 | 2.03(0.21) | (hG3)O6···(dC14)H42 | 2.03(0.19) |
| (hT4)H3···(rA13)N1 | 2.00(0.13) | (hT4)H3···(dA13)N1 | 1.98(0.12) |
| (hT4)O4···(rA13)H62 | 2.00(0.18) | (hT4)O4···(dA13)H62 | 2.05(0.21) |
| (hA5)N1···(rU12)H3 | 1.97(0.12) | (hA5)N1···(dT12)H3 | 1.98(0.13) |
| (hA5)H6A···(rU12)O4 | 2.11(0.26) | (hA5)H6A···(dT12)O4 | 2.10(0.27) |
| (hG6)H2B···(rC11)O2 | 1.87(0.11) | (hG6)H2B···(dC11)O2 | 1.90(0.13) |
| (hG6)H1···(rC11)N3 | 1.96(0.09) | (hG6)H1···(dC11)N3 | 1.97(0.09) |
| (hG6)O6···(rC11)H42 | 1.98(0.16) | (hG6)O6···(dC11)H42 | 1.98(0.17) |
| (hC7)O2···(rG10)H21 | 1.88(0.11) | (hC7)O2···(dG10)H21 | 1.88(0.12) |
| (hC7)N3···(rG10)H1 | 1.96(0.09) | (hC7)N3···(dG10)H1 | 1.95(0.09) |
| (hC7)H4A···(rG10)O6 | 1.98(0.17) | (hC7)H4A···(dG10)O6 | 1.97(0.17) |
| (hG8)H2B···(rC9)O2 | 1.93(0.15) | (hG8)H2B···(dC9)O2 | 1.94(0.17) |
| (hG8)H1···(rC9)N3 | 1.97(0.11) | (hG8)H1···(dC9)N3 | 2.03(0.29) |
| (hG8)O6···(rC9)H42 | 2.06(0.31) | (hG8)O6···(dC9)H42 | 2.20(0.61) |

[a] Values are in Å.

**Table 4.** Decomposition of Total Solvent Accessible Surface Areas into Contributions of the Base, Sugar, and Phosphate moieties and Polar and Hydrophobic Atoms[a]

| | base | | sugar | | phosphate | |
|---|---|---|---|---|---|---|
| | polar[b] | hydrophobic[c] | polar[b] | hydrophobic[c] | polar[a] | all |
| | | | HNA/DNA Duplex | | | |
| DNA strand | 209(6) | 189(10) | 133(7) | 403(11) | 260(7) | 1194(41) |
| HNA strand | 238(7) | 164(8) | 117(5) | 461(6) | 272(5) | 1252(31) |
| total | 447(10) | 353(15) | 250(9) | 864(12) | 532(8) | 2446(54) |
| | | | HNA/RNA Duplex | | | |
| RNA strand | 208(7) | 170(8) | 236(6) | 302(8) | 277(4) | 1193(33) |
| HNA strand | 237(6) | 167(10) | 113(5) | 464(6) | 266(5) | 1247(32) |
| total | 445(10) | 337(14) | 349(8) | 766(10) | 543(7) | 2440(49) |
| | | | HNA/RNA duplex[c] | | | |
| RNA strand | 208(7) | 171(8) | 134(5) | 382(7) | 277(4) | 1172(31) |
| HNA strand | 237(6) | 167(10) | 113(5) | 464(6) | 266(5) | 1247(32) |
| total | 445(10) | 338(14) | 247(7) | 846(10) | 543(7) | 2419(48) |

[a] Values are in Å$^2$. Standard deviations are in parentheses. [b] The solvent accessible surface area formed by O, N, and P atoms. [c] The solvent accessible surface area formed by C atoms. [d] Calculated from the HNA/RNA trajectory but with the van der Waals radius of the ribose 2′-OH group set to 0 Å.

Corongiu.[28] However, adjacent phosphate groups in the HNA and DNA/RNA strands are linked by single water molecules, where each bridging water is simultaneously hydrogen bonded to adjacent phosphate groups in the same oligonucleotide strand (Figure 8). This observation of single water molecules bridging adjacent phosphate groups is not only found in the two HNA/DNA and HNA/RNA complexes but is also observed in calculations performed on A-RNA.[27] The bridging water molecules, especially along the HNA strands, are positioned in the major grooves of the complexes. It is interesting to note that the density of the water molecules bridging the phosphates of the DNA strand in the HNA/DNA complex is approximately half the density of the waters along the RNA strand of the HNA/RNA complex, which are still visible at a contouring level of 8 times the expected water density. This may again be an indication of the higher flexibility of the DNA backbone in the HNA/DNA complex as compared to the RNA strand in the HNA/RNA duplex.

**(2) Major Groove.** Apart from the above-mentioned bridging waters between adjacent phosphates, additional hydration patterns found in the major groove include monodentate binding of water molecules to the N7 of HNA strand purines and to the keto oxygens and amino groups of purine and pyrimidine bases of the HNA chain (Figure 9). Again, as for the phosphate solvation pattern mentioned above, these additional major groove hydration schemes are observed in both the HNA/RNA and HNA/DNA duplexes.

**(3) Minor Groove.** The minor grooves of the HNA/DNA and HNA/RNA duplexes can be expected to be solvated distinctly due to the presence of O2′-hydroxyl groups in the RNA strand of the HNA/RNA complex and which are not present in HNA/DNA. Hence, minor groove solvation of HNA/DNA and HNA/RNA will be treated separately in the following. (i) HNA/DNA complex: The minor groove in this duplex is well-hydrated and involves interactions with both strands of the complex. Most water molecules located in the minor groove of the HNA/DNA duplex are well-defined, and density remains easily visible up to a contouring level of at least 6 times the expected water density. A chain of well-ordered water mol-

(28) Clementi, E.; Corongiu, G. *Biopolymers* **1979**, *18*, 2431−2450. (b) Clementi, E.; Corongiu, G. *J. Chem. Phys.* **1980**, *72*, 3979−3992.

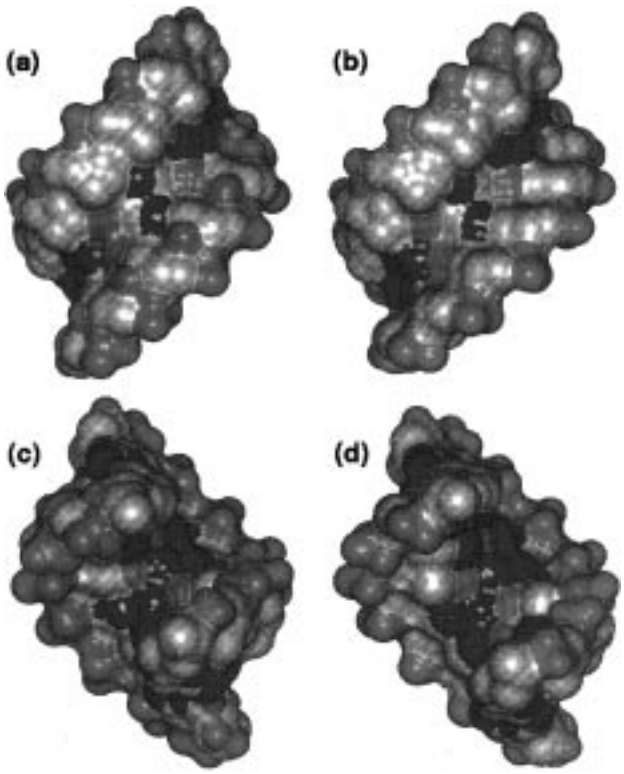


**Figure 7.** Color coding the total solvent accessible surface areas (SASAs) by their underlying atom type: N, blue; O, red; P, purple; and C, gray. (a) A view in the minor groove of the HNA/RNA complex. (b) The minor groove of HNA/DNA. (c) The major groove of HNA/RNA. (d) The major groove of HNA/DNA.

ecules forms a first hydration layer by bridging the O4′ deoxyribose ring oxygens of the DNA strand with the O2 or N3 atoms of the adjacent nucleobase. This layer of water molecules is linked to a second layer, which serves to complete the tetrahedral environment and which forms a linkage between the first water layer and the O2 or N3 atoms of the complementary anhydrohexitol nucleobases (Figure 10a). (ii) HNA/RNA complex: In the case of HNA/RNA, a minor groove hydration pattern similar to the HNA/DNA complex is observed *in casu* a well-defined chain of water molecules that links both strands of the duplex through contacts with the ribose O4′ atoms of the RNA strand and with the O2 or N3 base atoms of both strands (Figure 10b). As in the case of HNA/DNA, density remains visible up to a contouring level of at least 6 times the expected water density. However, due to the addition of the O2′ hydroxyl groups of the RNA chain, an additional hydration pattern is found as well. These O2′ hydroxyls contribute to the stabilization of water molecules in the minor groove by forming additional hydrogen bonds to the first hydration layer. Thus, the first layer of water molecules in the minor groove of the HNA/RNA complex not only bridges the O4′ atom and the O2 or N3 atom of the adjacent nucleobase but also bridges this O4′ atom and the O2′ hydroxyl group of the adjacent ribose (Figure 10b).

## Discussion

In general, HNA/RNA duplexes have higher melting temperatures than the corresponding HNA/DNA complexes, which is an indication of the increased stability of HNA/RNA as compared to HNA/DNA. Stability of a complex is determined by the free energy difference between the product and its reactants and hence requires knowledge of the free energy of each of these fractions. Although molecular dynamics by itself is not a suitable tool to study differences in free energy, it could be used to investigate differences in conformational energy, base-pair hydrogen bonding, hydration, and conformational flexibility. Hence, it is interesting to investigate whether the current calculations might help us to speculate about possible reasons for the increased stability of HNA/RNA as compared to HNA/DNA.

**Conformational Flexibility.** (a) There seems not to be a significant difference in backbone flexibility of the HNA strands in HNA/RNA and HNA/DNA, as evidenced by the similar standard deviations of each of the corresponding backbone torsion angles (Table 2). In addition, if one excludes residue hG1 from the comparison, the anhydrohexitol rings of the HNA strands in HNA/RNA and HNA/DNA remain all in a chair-like conformation, and the similar standard deviations on the pucker amplitude and phase angles $\theta$ and $\varphi$ are indicative of comparable flexibility of the anhydrohexitol rings as well (Table 2). Hence, conformational flexibility of the HNA chain is not likely a key factor in explaining the observed difference in stability of HNA/RNA versus HNA/DNA. (b) The RNA and DNA strands, on the other hand, display more variation in their flexibility, as indicated by the larger standard deviations on the DNA backbone torsion angles $\delta$, $\zeta$, and $\chi$ and puckering parameters as compared to the RNA values (Table 2 and Figure 6). However, it is unclear whether this difference in flexibility is correlated with the observed difference in stability or whether it is merely a characteristic inherently associated with the higher barrier of sugar repuckering of RNA as compared to DNA.[29] In this regard, the observation of a rigid RNA strand and a flexible DNA strand are also observed in calculations of a RNA/DNA hybrid structure,[27] indicating that this is not a characteristic of the HNA complexes alone.

**Base Pair Hydrogen Bonding.** The hydrogen bond distances and their standard deviations given in Table 3 are unable to discriminate between the HNA/RNA and HNA/DNA complexes in terms of relative stability. In each of the two duplexes, both strands interact strongly with each other through the formation of stable base-pair hydrogen bonds. Hence, the lower stability of the HNA/DNA complex in comparison to HNA/RNA is likely not due to sterical or geometrical reasons, as we would then expect to observe less stable hydrogen bonds in the case of HNA/DNA. In fact, there are no indications to believe that DNA strands are geometrically not capable of adopting an A-like geometry suitable to bind HNA strands, as there is abundant evidence of the spontaneous formation of A-type DNA double helices in low humidity conditions.[30]

**Solvation.** The total solvent accessible surface of both complexes is almost equal and fluctuates around 2430 Å$^2$ (Table 4). However, the minor groove of the duplexes, which in the case of the HNA/RNA duplex is lined with the 2′-OH groups of the ribose rings and which is relatively hydrophobic in the case of the HNA/DNA helix, forms the major difference between the two solvent accessible surfaces. As a consequence, the HNA/RNA complex has about 130 Å$^2$ more polar surface than the HNA/DNA system, which undoubtedly results in increased stabilization by solvent. In particular, upon formation of the HNA/DNA hybrid duplex, the complementary DNA strand is forced in a conformation in which its hydrophobic deoxyribose ring becomes fully exposed to the solvent present in the wide minor groove of all the atoms in the deoxyribose

(29) Olson, W. K.; Sussman, J. L. *J. Am. Chem. Soc.* **1982**, *104*, 270−278.

(30) Saenger, W. *Principles of nucleic acid structure*; Springer-Verlag: New York, 1984.

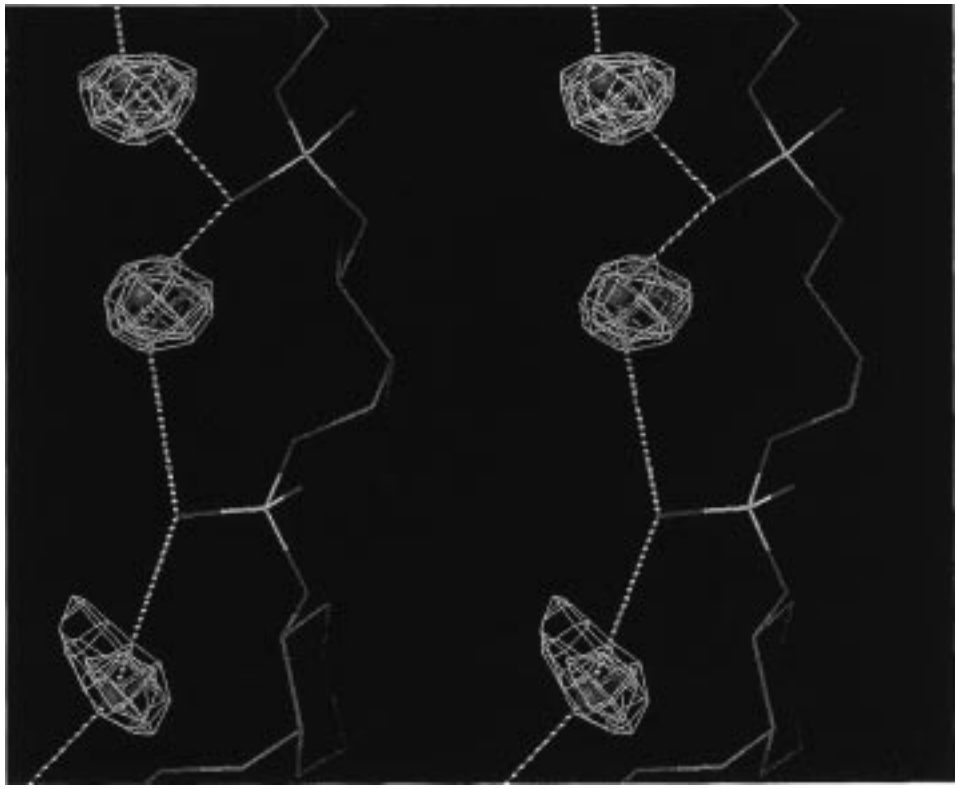

**Figure 8.** Stereo plot of the typical single water bridges between adjacent intrastrand phosphate groups. Shown are the backbone phosphates between anhydrohexitol residues hG3, hT4, and hA5 of the HNA/DNA complex, but similar arrangements are also observed for the phosphate groups of DNA strand and also of the HNA/RNA complex. Dotted lines denote possible hydrogen bonds. Density contouring levels are 8 (dark yellow), 6 (pale yellow), and 4 (purple) times the expected water density. Red dots are placed at positions of highest density.

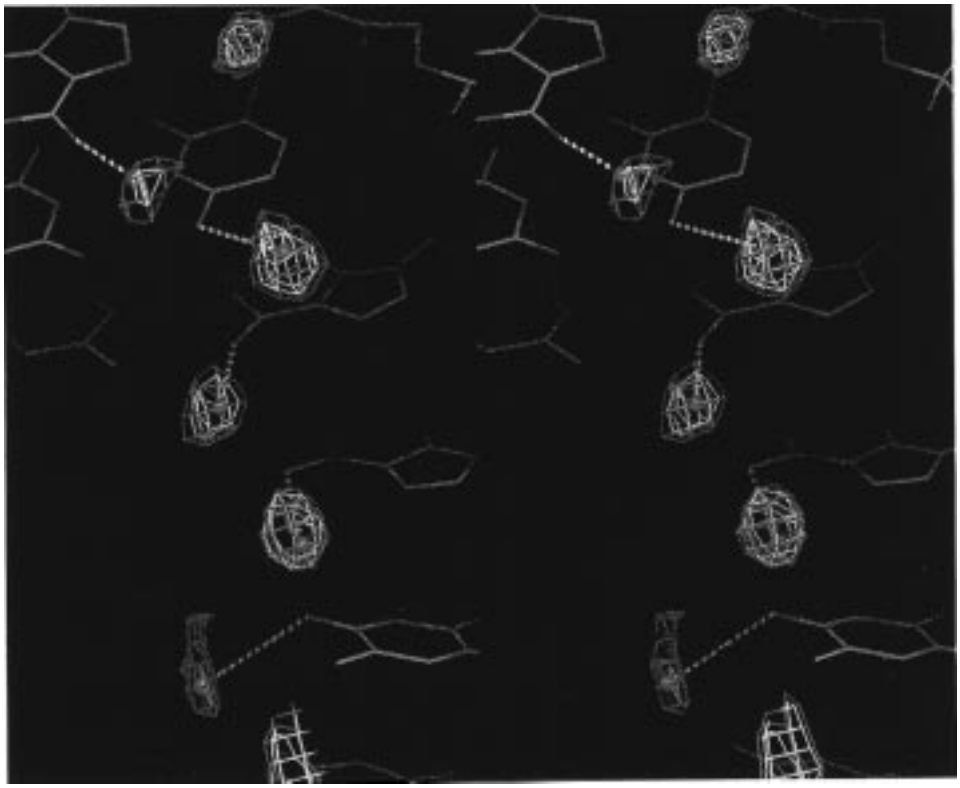

**Figure 9.** Stereo plot of residues hT4−hG8 of the HNA/DNA complex and their interaction with solvent waters in the major groove of the complex. A similar interaction pattern is observed for the HNA/RNA duplex. Hydrogen bonds are indicated by dotted white lines. Contouring is done at 4 (yellow) and 3 (red) times the expected water density. Red dots are placed at positions of highest density.

ring, only the O4′ atom interacts with solvent waters (Figure 10a). Clearly, this geometry, which is imposed by the structural rigidity of the HNA strand, is an unfavorable situation in terms of solvation. In this regard, it is interesting to note that, in stable double helices where at least one of the strands is a deoxyribose oligonucleotide, the minor groove is always narrower than the

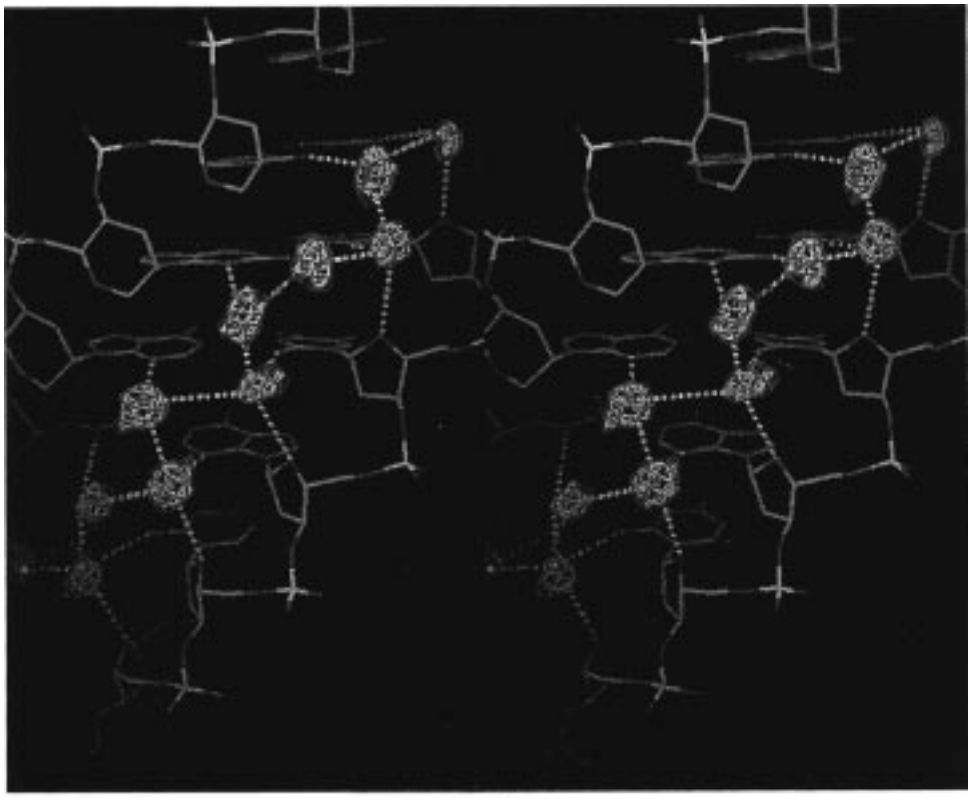

(a)

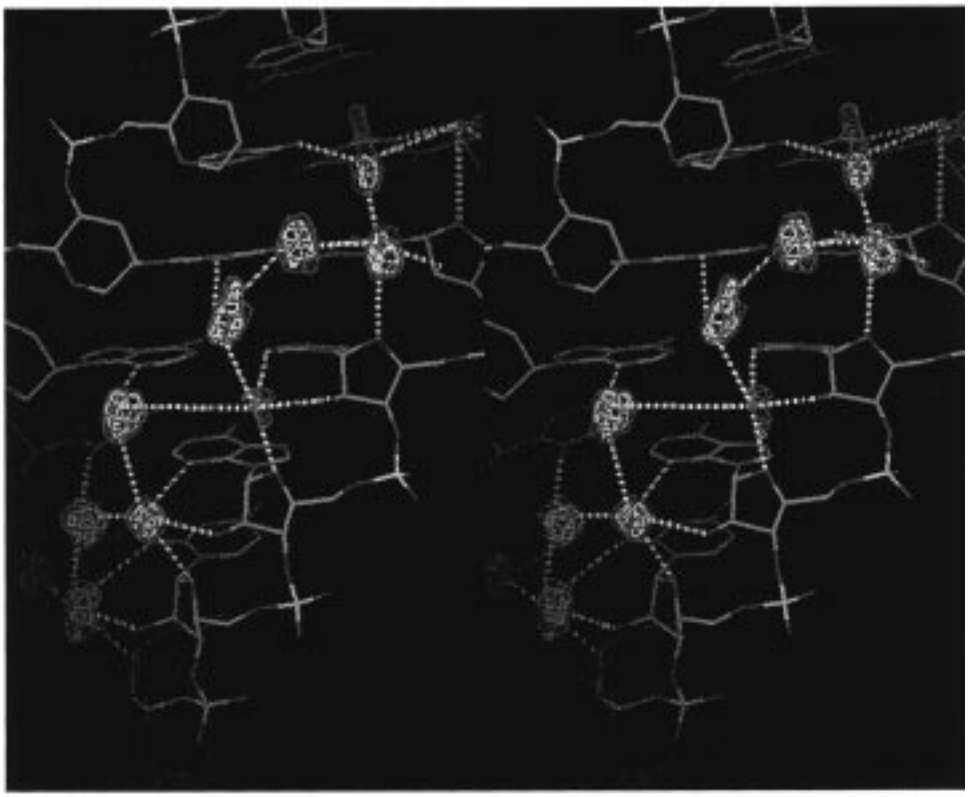

(b)

**Figure 10.** Stereo drawing of the minor grooves of the two complexes showing the well-defined hydration patterns in these grooves. Contouring is done at 4 (yellow) and 3 (red) times the expected water density. (a) HNA/DNA. (b) HNA/RNA.

12 Å calculated here for the HNA/DNA hybrid. In particular, minor groove widths around ∼6 Å are typical for B-type double helical DNA, while for A-type DNA, which is only found in high salt or crystalline conditions, values of ∼11 Å have been published.[30] In addition, minor groove widths for RNA/DNA hybrids are in the range of 8−11 Å.[31,32]

Compared to the HNA/DNA situation, minor groove solvation is clearly more optimal in the case of HNA/RNA. Just as for HNA/DNA, the RNA strand is also held in a A-like conformation when complexed to HNA, and the complex is also characterized by a wide minor groove that is fully accessible to solvent. Not only the distribution of water molecules in the minor groove of HNA/RNA is identical to the pattern in HNA/DNA, but also the density of the minor groove water molecules is very similar in both cases. However, the presence of 2′-OH groups in the RNA strand renders the minor groove of the HNA/RNA duplex significantly more hydrophilic as compared to the HNA/DNA system. Not only the O4′ atoms but also the 2′-OH groups of the ribose rings are all involved in well-defined interactions with water molecules (Figure 10b). Therefore, minor groove solvation might be an important factor which could, at least in part, explain the relative stability of HNA/RNA systems as compared to HNA/DNA. If this would be the case, then double helical stability could be improved by designing oligonucleotides with increased minor groove solvation. Of course, other factors, such as entropy effects, are likely also important in explaining the relative stabilities, but these are difficult to estimate from molecular dynamics calculations.

## Conclusions

Hexitol nucleic acids are intriguing structures as they belong to the group of oligomers that hybridize strongly and selectively with natural RNA. They show stronger base pairing as well as a greater selectivity of pairing with ribooligonucleotides than the pairing found between natural nucleic acids. The reason for the higher stability of HNA/RNA duplexes as compared to the HNA/DNA complexes was investigated here using molecular dynamics. The selection of the starting conformation used to carry out the modeling experiments was based on NMR analysis of a HNA dimer. Both complexes (HNA/RNA and HNA/DNA) show an A-type geometry and very similar hydrogen bonding patterns between base pairs. Although it is certainly not the only factor determining complex stability, minor groove solvatation contributes to a considerable extent to duplex stabilization and might explain, at least in part, the relative stability of HNA/RNA versus HNA/DNA. To further explore the influence of hydration on the stability of oligonucleotide complexes with a six-membered carbohydrate mimic in the backbone structure, we are currently modeling and synthesizing the D-mannitol and D-altritol analogues of the aforementioned hexitol nucleic acids. These studies might lead to more efficient antisense constructs, functioning by sterically blocking the RNA target.

**Acknowledgment.** This work was supported by a grant of the K.U. Leuven (GOA 97/11). We thank J. Rozenski for mass spectrometric analysis. A.V.A. is a research associate, and E.L. is an aspirant of the Belgian National Fund of Scientific Research. We are grateful to A. De Bruyn and H. van Halbeek for their help in interpreting NMR data. We thank M. Vandekinderen for editorial help.

JA973721F

(31) Horton, N. C.; Finzel, B. C. *J. Mol. Biol.* **1996**, *264*, 521−533.
(32) Arnott, S.; Chandrasekaran, R.; Millane, R. P.; Park, H. S. *J. Mol. Biol.* **1986**, *188*, 631−640.
(33) Cremer, D.; Pople, J. A. *J. Am. Chem. Soc.* **1975**, *97*, 1354−1358.
(34) Altona, C.; Sundaralingam, M. *J. Am. Chem. Soc.* **1972**, *94*, 8205−8212.